JSR Publications

Available Online

J. Sci. Res. **13** (1), 31-45 (2021)

JOURNAL OF SCIENTIFIC RESEARCH

www.banglajol.info/index.php/JSR

Study of Carbon Nanotubes with a Casson Fluid in a Vertical Channel of Porous Media under MHD and Dufour Effect

S. Hazarika, S. Ahmed*

Department of Mathematics, Rajiv Gandhi University, Itanagar, Arunachal Pradesh, 791112, India

Received 9 June 2020, accepted in final revised form 17 September 2020

Abstract

An analysis is conducted to investigate the problem of heat/mass transfer in MHD free convective flow of Casson-fluid in a vertical channel embedded with saturated porous medium past through carbon nanotubes in the form of single-wall carbon nanotubes (SWCNTs) and multiple-wall carbon nanotubes (MWCNTs) with engine oil as base fluid. In this article, the impact of CNT's on velocity, temperature, shear stress and rate of heat transfer of the nanofluid has been investigated and studied graphically for the effects of different key physical parameters involved. The validity of this flow model is presented and is found satisfactory agreement with published results. The results state that, fluid velocity accelerates for greater values of Casson parameter and nanoparticles volume fraction, while thermal radiation (R) and heat generation (Q) assume a significant role in CNT's. Applications of this study arise in broad area of science and engineering such as thermal conductivity, energy storage, biomedical applications, air and water filtration, fibers and fabrics.

Keywords: Casson fluid; SWCNT; MWCNT; Dufour effect.

doi: http://dx.doi.org/10.3329/jsr.v13i1.47458 J. Sci. Res. **13** (1), 31-45 (2021)

1. Introduction

Recently, an interest of extensive research has given towards the investigation of carbon nanotubes and its various applications for their small dimensions, high thermal conductivity and unique architecture and for having huge potential in nanotechnology, nano-medicine as biocompatible, air refinement scheme, mechanical compound materials, superfluous strong filaments, sensors devices, storage of gas, bio-sensors and many more. CNTs are generally comprised of pure carbon and belongs to the group of fullerenes (C60), and these are accessible in different geometrical shapes like tubes, spherical, or ellipsoidal, which are mainly classified into two types such as single-walled carbon nanotubes (SWCNTs) and multi-walled carbon nanotubes (MWCNTs) depending upon the structure.

Now days, CNTs have been considered as an ideal nano-carrier in the field of science and engineering. Many researchers [1–6] have paid an important attention on the CNTs

* *Corresponding author*: sahin.ahmed@rgu.ac.in

with various effects such as heat transfer, thermal conductivity, thermal radiations, porous medium and so on. Aman *et al.* [7] studied heat transfer enhancement in free convection flow of CNTs Maxwell nanofluids with four different types of molecular liquid. Convective heat transfer in MHD slip flow over a stretching surface in the presence of carbon nanotubes is discussed by Haq *et al.* [8]. Khan *et al.* [9] studied the slip flow of Eyring-Powell nanoliquid film which contains nanoparticles of graphene. Three-dimensional nanofluid flow with heat and mass transfer analysis over a linear stretching surface with convective boundary conditions is illustrated by Khan *et al.* [10]. Also, Reddy *et al.* [11] addressed MHD boundary layer flow, heat and mass transfer analysis over a rotating disk of Cu-water and Ag-water nanofluid with chemical reaction through porous medium.

Further, Kandasamy *et al.* [12] explores the influence of various effects like Soret, Dufour, chemical reaction, heat source on free convective heat and mass transfer. Heat transfer of Cu-water nanofluid in an enclosure with a heat sink and discrete heat source is researched by Hassan [13]. Also, Reddy *et al.* [14] discussed the effects of Soret and Dufour on MHD convective flow of Al_2O_3–water and TiO_2–water nanofluids in a stretching sheet saturated by porous media with heat generation/absorption.

Moreover, it is important to note here that numerous fluids of industrial importance are non-Newtonian because of their applications in petroleum drilling, polymer engineering, certain separation processes, food manufacturing and some other modern procedures. Due to the nonlinearity between the stress and the rate of strain for non-Newtonian fluids, it is hard to explain every one of those properties of a few non-Newtonian fluids in a single constitutive equation. This has approached the consideration of researcher to examine the flow dynamics of non-Newtonian fluids. Consequently, several non-Newtonian fluid models have been proposed depending on various physical properties. The most well-known among these fluids is the Casson fluid. Casson model is introduced by Casson to predict flow behavior of pigment oil suspensions of the printing ink type, which is a shear thinning liquid assumed to have infinite viscosity at zero rate of shear and gives stress below which no flow occurs. Jelly, tomato sauce, honey, soup, engine oil, human blood etc. are the examples of Casson fluids [15]. Mukhopadhyay *et al.* [16] discussed the exact solutions for the flow of Casson fluid over a stretching surface with transpiration and heat transfer effects. Analysis of Casson fluid flow over a vertical porous surface with chemical reaction in the presence of magnetic field is observed by Arthur *et al.* [17]. Hayat *et al.* [18] illustrated the mixed convection flow of Casson nanofluid over a stretching sheet with convectively heated chemical reaction and heat source/sink. Recently many useful researches have been developed by various researchers [22-33] about heat transfer through convective boundary conditions, heat source/ sink, radiation effect and chemical reaction of nanofluid/ nanotubes. Kalita *et al.* [36,37] discussed the effect of various emerging parameter on CNT and nanofluids with different shapes. Many recent researches [19-21,34,35,37-39] have been done on nanofluids with its powerful effect and found useful conclusions.

In this article, engine oil is used as base fluid inside CNTs. The study of CNT with Casson fluid is considered as one of the important problems because of its development in many engineering problems. Carbon nanotubes can be used for the potential applications, structural evaluation, which have exceptional tensile strength and extraordinary electrical conductivity, also they can be chemically modified.

This research is aimed to investigate the impact of CNT's in a vertical porous channel filled with Casson fluid (engine oil) and also this study enlightens the effects of heat/mass flux, diffusion thermo, Casson parameter, CNT volume fraction, magnetic drag force and Schmidt parameter on velocity, temperature, shear stresses and rate of heat transfer for different CNT's with special emphasis on thermal radiation. All the relevant investigative findings of the embedded parameters are graphically displayed

2. Mathematical Formulation

We consider an electrically conducting fluid in a vertical channel of width a, and static walls at $y = 0$ and $y = a$ with a uniform magnetic field of strength B_0 applying transversely to the channel. This MHD flow is assumed to be incompressible and unsteady with heat and mass transport in Casson fluid (engine oil) containing SWCNT and MWCNT embedded in a saturated porous medium and are presented in Figs. 1 and 2.

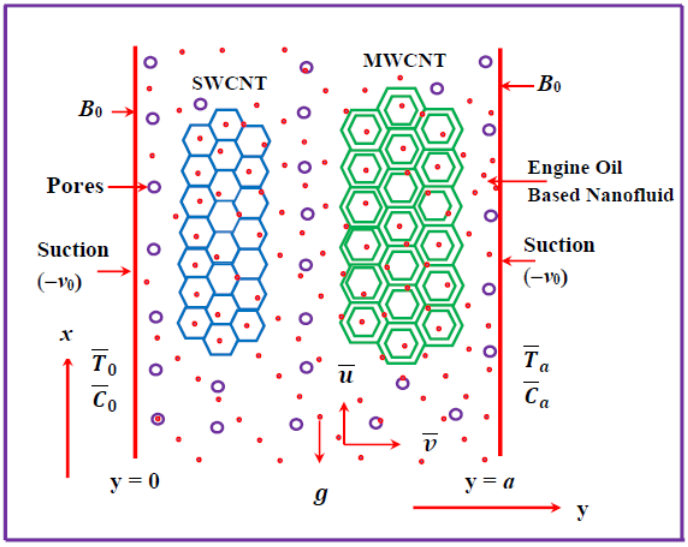

Fig. 1. Physical configuration and coordinate system [19,28,29,32].

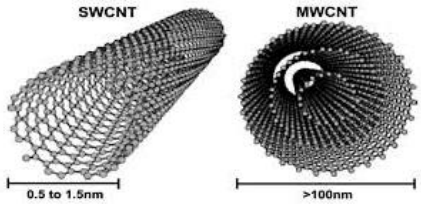

Fig. 2. Distribution of SWCNT and MWCNT [19,34,35].

Under the assumptions of [29] and [32], the boundary layer equations for CNTs in a vertical channel of Casson fluid are given by

$$\frac{\partial \bar{v}}{\partial \bar{y}} = 0\,, \tag{1}$$

$$\rho_{nf}\frac{\partial \bar{u}}{\partial \bar{t}} = \begin{Bmatrix} -\frac{\partial \bar{p}}{\partial \bar{x}} + \mu_{nf}\left(1+\frac{1}{\gamma}\right)\frac{\partial^2 \bar{u}}{\partial \bar{y}^2} - \left(\sigma_{nf}B_0^2 + \frac{\mu_{nf}}{\bar{K}_1}\right)\bar{u} \\ +(\rho\beta)_{nf}g(\bar{T}-\bar{T}_a) + (\rho\beta)_{nf}g(\bar{C}-\bar{C}_a) \end{Bmatrix}, \tag{2}$$

$$\left(\rho C_p\right)_{nf}\frac{\partial \bar{T}}{\partial \bar{t}} = -\frac{\partial \bar{q}_r}{\partial \bar{y}} + \kappa_{nf}\frac{\partial^2 \bar{T}}{\partial \bar{y}^2} - Q_0(\bar{T}-\bar{T}_a) + \frac{D_m K_T}{C_s}\frac{\partial^2 \overline{C}}{\partial \overline{y}^2}\,, \tag{3}$$

$$\frac{\partial \overline{C}}{\partial \bar{t}} = D_m\frac{\partial^2 \overline{C}}{\partial \overline{y}^2} - \overline{K}_r(\bar{C}-\bar{C}_a)\,, \tag{4}$$

Eq. (1) gives: $\bar{v} = -v_0 \;\; (v_0 > 0)$,

where $\bar{u}$ and $\bar{v}$ are the velocity components in the $\bar{x}$ and $\bar{y}$ directions respectively, v_0 is the suction velocity to the plate, $\bar{T}$ is the temperature, $\bar{C}$ is the concentration of the nanofluid , $\bar{T}_a \; and \; \bar{C}_a$ are the temperature and concentration of the nanofluid at wall $y = a$, B_0 is the uniform magnetic field strength, γ is the Casson parameter, σ is the electrical conductivity, C_p is the specific heat at constant pressure, $\bar{p}$ is the dimensional pressure, Q_0, dimensional heat source, D_m is the species diffusivity, $\overline{K}_1$ is the permeability of the porous medium, $\overline{K}_r$is a chemical reaction parameter; and μ, ρ, κ and ρC_p are the dynamic viscosity, density, thermal conductivity and heat capacitance, respectively. Here suffices *CNT, nf, f* are the carbon nanotubes, nanofluid and base fluid respectively.

For nanofluids, the static part in the effective thermal conductivity κ_{nf} and the effective viscosity μ_{nf} are derived from Maxwells *et al.* [22], Brinkmans *et al.* [20] and Xuan *et al.* [21] models and are defined as (here ϕ is the volume fraction of carbon nanotubes).

$$\left\{\begin{array}{c} \mu_{nf} = \dfrac{\mu_f}{(1-\phi)^{2.5}}\,, \;\; (\rho)_{nf} = (1-\phi)(\rho)_f + \phi(\rho)_{CNT}\,, \\ (\rho\beta)_{nf} = (1-\phi)(\rho\beta)_f + \phi(\rho\beta)_{CNT}\,, \left(\rho C_p\right)_{nf} = (1-\phi)\left(\rho C_p\right)_f + \phi\left(\rho C_p\right)_{CNT}\,, \\ \dfrac{\kappa_{nf}}{\kappa_f} = \dfrac{(1-\phi)+2\phi\left(\dfrac{\kappa_{CNT}}{\kappa_{CNT}-\kappa_f}\right)ln\dfrac{\kappa_{CNT}+\kappa_f}{2\kappa_f}}{(1-\phi)+2\phi\left(\dfrac{\kappa_f}{\kappa_{CNT}-\kappa_f}\right)ln\dfrac{\kappa_{CNT}+\kappa_f}{2\kappa_f}}, \sigma_{nf} = \sigma_f\left[1+\dfrac{3(\sigma-1)\phi}{(\sigma+2)-(\sigma-1)\phi}\right] \end{array}\right\} \tag{5}$$

The radiative heat flux [19,29,32] is given by,

$$\frac{\partial \overline{q}}{\partial \overline{y}} = -4\alpha^2\left(\overline{T} - \overline{T}_a\right) \tag{6}$$

where , α is an absorbent coefficient and $\overline{q}$ is the dimensional radiative heat flux

Let us introduce the non-dimensional parameters:

$$\left\{\begin{array}{c} x = \frac{\overline{x}}{d}\ ,\ y = \frac{\overline{y}}{d}\ ,\ u = \frac{\overline{u}}{U_0}\ ,\ \ t = \frac{\overline{t}U_0}{d}\ ,\theta = \frac{\overline{T}-\overline{T}_a}{\overline{T}_0-\overline{T}_a}, \psi = \frac{\overline{C}-\overline{C}_a}{\overline{C}_0-\overline{C}_a}, \\ p = \frac{\overline{p}d}{\mu_f U_0}, \omega = \frac{\overline{\omega}d}{U_0}\ , \frac{\partial p}{\partial x} = \lambda\, exp(i\omega t)\ , \mathrm{Re} = \frac{U_0 d}{\nu_f}\ , \\ \mathrm{M}^2 = \frac{\sigma_f d^2 B_0^2}{\mu_f}\ , \mathrm{K} = \frac{\overline{K}_1}{d^2}, \mathrm{Gr} = \frac{d^2 g\beta_f(\overline{T}_0-\overline{T}_a)}{U_0\mu_f}\ , \lambda_n = \frac{\kappa_{nf}}{\kappa_f}\ , \\ \mathrm{Gm} = \frac{d^2 g\beta_f(\overline{C}_0-\overline{C}_a)}{U_0\mu_f}\ ,\ \mathrm{Q} = \frac{Q_0 d^2}{\kappa_f}\ , \mathrm{Pe} = \frac{U_0 d(\rho C_p)_f}{\kappa_f}\ , \\ \mathrm{R}^2 = \frac{4d^2\alpha^2}{\kappa_f}, \mathrm{Du} = \frac{D_m K_T(\overline{C}_0-\overline{C}_a)}{\kappa_f C_s(\overline{T}_0-\overline{T}_a)}, \mathrm{Sc} = \frac{U_0 d}{D_m}, Kr = \frac{\overline{K}_r d}{U_0} \end{array}\right\} \tag{7}$$

Here d is the distance between the wall; $x\ and\ y$ are the coordinate system; U_0 is the reference velocity; $u,\ \theta,\ \psi$ and t are the dimensionless velocity, temperature, concentration and time respectively. p is the dimensionless pressure, ω is angular velocity, λ is the perturbation constant. $Re, M, K, Gr, Gm, \lambda_n, Q, Pe, R, Du, Sc$ and Kr represent Reynold's number, magnetic number, porosity parameter, thermal Grashof number, Grashof number due to mass transfer, ratio of thermal conductivity of nanofluid to that of base fluid, heat source, Peclet number, radiation parameter, Dufour effect, Schmidt number and chemical reaction parameter respectively.

The boundary conditions are given by:

$$\left\{\begin{array}{ll} \bar{u}(0,t) = 0, & \bar{u}(a,t) = 0 \\ \bar{T}(0,t) = T_0, & \bar{T}(a,t) = T_a \\ \bar{C}(0,t) = C_0, & \bar{C}(a,t) = C_a \end{array}\right\} \tag{8}$$

With the help of (5) – (6), the eqs (2) – (4) reduce to the dimensionless form:

$$\phi_1 \mathrm{Re}\frac{\partial u}{\partial t} = \varepsilon\lambda exp(i\omega t) + \phi_2\left(1+\frac{1}{\gamma}\right)\frac{\partial^2 u}{\partial y^2} - \left(\mathrm{M}^2\phi_3 + \frac{\phi_2}{\mathrm{K}}\right)u + \phi_4 \mathrm{Gr}\,\theta + \phi_4 \mathrm{Gm}\,\psi \tag{9}$$

$$\phi_5 \mathrm{Pe}\frac{1}{\lambda_n}\frac{\partial \theta}{\partial t} = \frac{\partial^2 \theta}{\partial y^2} + \left(\frac{\mathrm{R}^2}{\lambda_n} - \frac{\mathrm{Q}}{\lambda_n}\right)\theta + \frac{\mathrm{Du}}{\lambda_n}\frac{\partial^2 \psi}{\partial y^2} \tag{10}$$

$$\frac{\partial \psi}{\partial t} = \frac{1}{\mathrm{Sc}}\frac{\partial^2 \psi}{\partial y^2} - Kr\psi \tag{11}$$

The dimensionless forms of (8) are

$$\left.\begin{array}{ll} u(0,t)=0, & u(1,t)=0 \\ \theta(0,t)=1, & \theta(1,t)=0 \\ \psi(0,t)=1, & \psi(1,t)=0 \end{array}\right\} \tag{12}$$

The eqs (9) – (11) may be re-written as

$$a_0\frac{\partial u}{\partial t}=\varepsilon\lambda exp(i\omega t)+a_1\frac{\partial^2 u}{\partial y^2}-a_2u+a_3\theta+a_4\psi \tag{13}$$

$$b_0^2\frac{\partial\theta}{\partial t}=\frac{\partial^2\theta}{\partial y^2}+b_1^2\theta+b_2\frac{\partial^2\psi}{\partial y^2} \tag{14}$$

$$\frac{\partial\psi}{\partial t}=\frac{1}{Sc}\frac{\partial^2\psi}{\partial y^2}-Kr\psi \tag{15}$$

To solve the eqs. (13) – (15) with the boundary conditions (11), the perturbed solutions are taken of the forms:

$$f(y,t)=f_0(y)+\varepsilon\, e^{i\omega t}f_1(y)+O(\varepsilon^2)\ldots\ldots \tag{16}$$

where f stands for $u\,,\theta\ or\ \psi$ and $\varepsilon << 1$.

On using the eqs. (16) into eqs. (13) – (15), we obtain the following system of ordinary differential equations,

$$\frac{d^2u_0(y)}{dy^2}-\ a_5^2u_0(y)=-a_6\theta_0(y)--a_7\psi_0(y) \tag{17}$$

$$\frac{d^2u_1(y)}{dy^2}-\ a_8^2u_1(y)=-\lambda_1-a_6\theta_1(y)-a_7\psi_1(y) \tag{18}$$

$$\frac{d^2\theta_0(y)}{dy^2}+\ b_1^2\theta_0(y)=-b_2\frac{d^2\psi_0(y)}{dy^2} \tag{19}$$

$$\frac{d^2\theta_1(y)}{dy^2}+\ b_2^2\theta_1(y)=-b_2\frac{d^2\psi_1(y)}{dy^2} \tag{20}$$

$$\frac{d^2\psi_0(y)}{dy^2}-d_1^2\psi_0(y)=0 \tag{21}$$

$$\frac{d^2\psi_1(y)}{dy^2}-d_2\psi_0(y)=0 \tag{22}$$

The transformed boundary conditions (12) are

$$\left.\begin{array}{llll} u_0(0)=0\,, & u_0(1)=0\,, & u_1(0)=0\,, & u_1(1)=0 \\ \theta_0(0)=1\,, & \theta_0(1)=0\,, & \theta_1(0)=0\,, & \theta_1(1)=0 \\ \psi_0(0)=1\,, & \psi_0(1)=0, & \psi_1(0)=0\,, & \psi_1(1)=0 \end{array}\right\} \tag{23}$$

The solutions of the eqs. (16) to (21) the under boundary conditions (22) yield to

$$u(y,t) = \begin{Bmatrix} (p_1 - p_2)e^{a_5 y} + p_2 e^{-a_5 y} + D\sin(b_1 y) + E\cos(b_1 y) - Je^{d_1 y} \\ +Ge^{-d_1 y} + \varepsilon\, e^{i\omega t}\left(p_4 e^{a_8 y} + p_3 e^{-a_8 y} + \frac{\lambda_1}{a_8^2}\right) \end{Bmatrix} \quad (24)$$

$$\theta(y,t) = C\sin(b_1 y) + C_1\cos(b_1 y) + B\, e^{d_1 y} + B_1\, e^{-d_1 y} \quad (25)$$

$$\psi(y,t) = (1-A)e^{-d_1 y} + A\, e^{d_1 y} \quad (26)$$

Shear Stress

The shear stresses in terms of skin-frictions in non-dimensional form at $y = 0$ and $y = 1$are as follows:

$$\tau_0 = \left.\frac{\partial u}{\partial y}\right|_{y=0} = \begin{Bmatrix} (p_1 - p_2)a_5 - p_2 a_5 + Db_1 - Jd_1 \\ -Gd_1 + \varepsilon\, e^{i\omega t}\{p_4 a_8 - p_3 a_8\} \end{Bmatrix} \quad (27)$$

$$\tau_1 = \left.\frac{\partial u}{\partial y}\right|_{y=1} = \begin{Bmatrix} (p_1 - p_2)a_5 e^{a_5 y} - p_2 a_5 e^{-a_5 y} + Db_1\cos(b_1) - E\, b_1 sin(b_1) \\ -Jd_1 e^{d_1 y} - Gd_1 e^{-d_1 y} + \varepsilon\, e^{i\omega t}(p_4 a_8 e^{a_8 y} - p_3 a_8 e^{-a_8 y}) \end{Bmatrix} \quad (28)$$

Rate of Heat Transfer

The rate of heat transfer in non-dimensional form at $y = 0$ and $y = 1$are as follows:

$$Nu_0 = \left.\frac{\partial \theta}{\partial y}\right|_{y=0} = \{Cb_1 + Bd_1 - B_1 d_1\} \quad (29)$$

$$Nu_1 = \left.\frac{\partial \theta}{\partial y}\right|_{y=1} = \begin{Bmatrix} Cb_1\cos(b_1) + C_1 b_1\, sin(b_1) + \\ Bd_1 exp(d_1) - B_1 d_1 exp(-d_1) \end{Bmatrix} \quad (30)$$

3. Validity and Accuracy

The accuracy of the present CNT model is verified by comparing the results with published results illustrated by Aman *et al*. [19] at $\mathrm{Gm} = 0$ and $\mathrm{Gm} = 2$ for velocity and at $\mathrm{Du} = 0$ and $\mathrm{Du} = 5$ for temperature. The comparisons of the velocity and temperature for CNT-engine oil are presented in Tables 1 and 2.

Table 1. Velocity profile for Gm in CNT for Engine oil at $\lambda = 1, t = 2, \omega = 2, \mathrm{R} = 2, \mathrm{Gr} = 2, \mathrm{K} = 0.01, \mathrm{Re} = 2, \mathrm{Pe} = 3.5, \mathrm{Sc} = 0.78, Kr = 0.05, \mathrm{M} = 2, \mathrm{Du} = 2, \mathrm{Q} = 2, \sigma = 0.8, \gamma = 0.5, \alpha = 1, \varepsilon = 0.001$.

	Aman *et al.* [19] at $Gm = 0$			Present work at $Gm = 5$		
y	$\phi = 0.05$	$\phi = 0.1$	$\phi = 0.15$	$\phi = 0.05$	$\phi = 0.1$	$\phi = 0.15$
0.0	0	0	0	0	0	0
0.2	2.027	3.440	4.409	3.871	6.665	8.610
0.4	2.162	3.630	4.623	4.056	6.942	8.941
0.6	1.638	2.725	3.453	3.028	5.157	6.625
0.8	0.864	1.429	1.804	1.582	2.686	3.444
1.0	0	0	0	0	0	0

Table 2. Temperature profile for Q in CNT for engine oil $\lambda = 1, t = 2, \omega = 2, \mathrm{Q} = 2, \mathrm{R} = 2, \sigma = 0.8, \gamma = 0.5, \alpha = 1, \mathrm{Pe} = 3.5$.

	Aman et al. [19] at Du = 0			Present work at Du = 5		
y	$\phi = 0.05$	$\phi = 0.1$	$\phi = 0.15$	$\phi = 0.05$	$\phi = 0.1$	$\phi = 0.15$
0.0	1	1	11	1	1	1
0.2	0.8688	0.8474	0.8352	0.9097	0.8727	0.8527
0.4	0.6935	0.6641	0.6474	0.7488	0.6981	0.6708
0.6	0.4829	0.4566	0.4417	0.5317	0.4865	0.4623
0.8	0.2477	0.2325	0.2239	0.2758	0.2497	0.2357
1.0	0	0	0	0	0	0

The present model is validated and accurate through the analysis of Tables 1 and 2.

4. Results and Discussion

All the numerical computations have been done through Table 3 for the properties of engine oil, SWCNTs and MWCNTs. The plotted curves are drawn for human blood-based nanofluid with SWCNTs and MWCNTs on velocity, temperature and skin friction of Casson-nanofluid. Default values of various parameters, which have been used to graphically analyze the effectiveness of the model are as follows: $\lambda = 1, t = 2, \omega = 2, \mathrm{R} = 2, \mathrm{Gr} = 2, \mathrm{K} = 0.01, \mathrm{Re} = 2, \mathrm{Pe} = 3.5, \mathrm{Sc} = 0.78, \mathrm{K_r} = 0.05, \mathrm{M} = 2, \mathrm{Du} = 2, \mathrm{Q} = 2, \sigma = 0.8, \gamma = 0.5, \alpha = 1, \varepsilon = 0.001$.

Table 3. Thermophysical properties of Engine oil and CNTs.

	ρ (Kg/m^3)	C_p (J/KgK)	κ (W/mk)	σ (S/m)	$\beta \times 10^5$ (K^{-1})
Engine oil	884	1910	0.144	0.8	0.18
SWCNT's	2600	425	6600	$10^6 - 10^7$	27
MWCNT's	1600	796	3000	1.9×10^{-4}	44

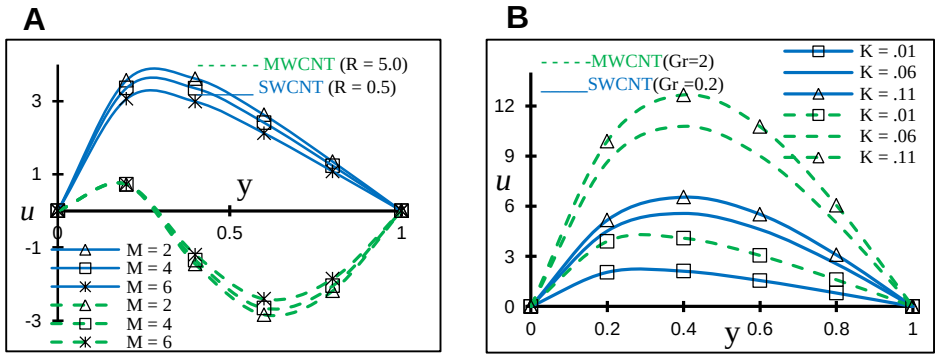

Fig. 3. A) Impact of M on velocity profile (u) for MWCNT (R = 5) and SWCNT (R = 0.5). B) Impact of K on velocity profile (u) for MWCNT (Gr = 2) SWCNT (Gr = 0.2).

Fig. 3A describes the behavior of magnetic number on nanofluid velocity. It shows that the augmented values of M reduces the nanofluid motion, because a resistive force like Lorentz is generated during the motion of the electrically conducting nanofluid which retards the motion. Moreover, maximum negative values of u is seen for the case of MWCNT when the thermal radiation is greater (R = 5) and hence back flow may occur in the channel. The impact of SWCNTs is more dominant than MWCNTs.

Fig. 3B displays the influences of K and Gr on nanofluid velocity (u). It is observed that the behaviour of velocity is elevated for all greater values of K and Gr in the middle of the channel for both MWCNT and SWCNT. However, when K increases, physically the resistance of the porous medium is minimized for which momentum boundary layer of nanofluid increases and ultimately escalates the velocity for both SWCNTs and MWCNTs. These effects are natural phenomenon in physical prospects.

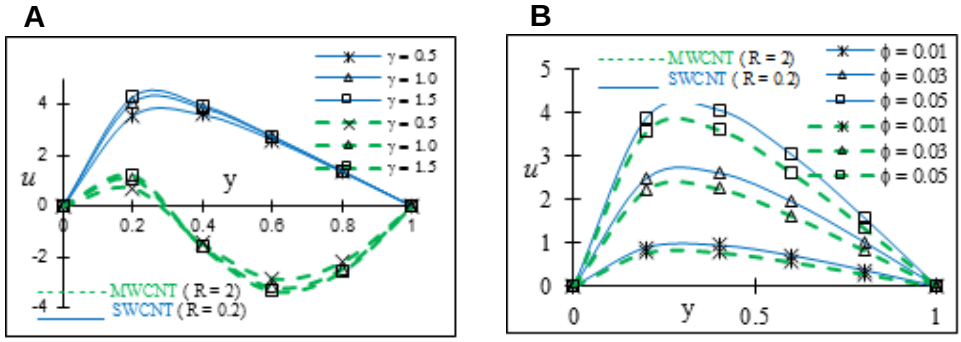

Fig. 4. A) Impact of γ on velocity profile (u) for MWCNT (R = 2) and SWCNT (R = 0.2). B) Impact of ϕ on velocity profile for MWCNT (R = 2) and SWCNT (R = 0.2).

Fig. 4A depicts the influence of γ and R on u. Increasing behaviour is observed in u with augmented values of (γ). It is seen that u has higher value for the case of SWCNT than MWCNT and for $y \geq 0.2$, opposite behaviour is observed for MWCNT (R = 5) and back flow may occur.

Fig. 4B illustrates the effect of ϕ on u at higher and lower values of R. In the region $0 \leq y \leq 1$, increasing behavior of u is observed with enhances in ϕ. The behavior of u is more dominant in MWCNT than SWCNT. This is due to the fact that an increase in ϕ indicates a raise in the thermal conductivity of the CNTs nanofluid and for which the viscosity raises and hence flow velocity enhanced.

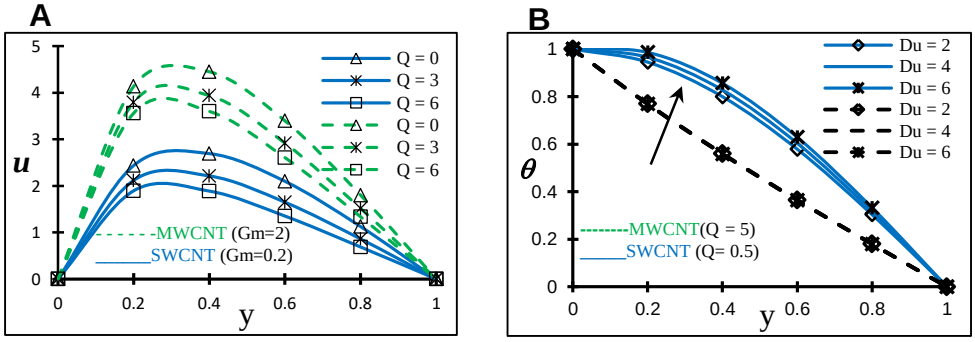

Fig. 5. A) Impact of Q on velocity profile (θ) for MWCNT (Gm = 2) and SWCNT (Gm = 0.2). B) Impact of Du on temperature profile (θ) for MWCNT (Q = 5) and SWCNT (Q = 0.5).

The effects of Q and mass Gm on velocity for CNTs' are shown in Fig. 5A. It is observed that velocity is elevated for smaller Q and the flow motion in MWCNT is more dominant than SWCNT, that is, velocity is accelerated for greater values of Gm.

In Fig. 5B all the profiles of θ are sharply elevated due to the increasing effect of diffusion thermo parameter, while heat generation parameter is reducing the fluid temperature in the channel. However, SWCNT is more dominant than that of MWCNT and more heat is conducted near the plate $y = 0$.

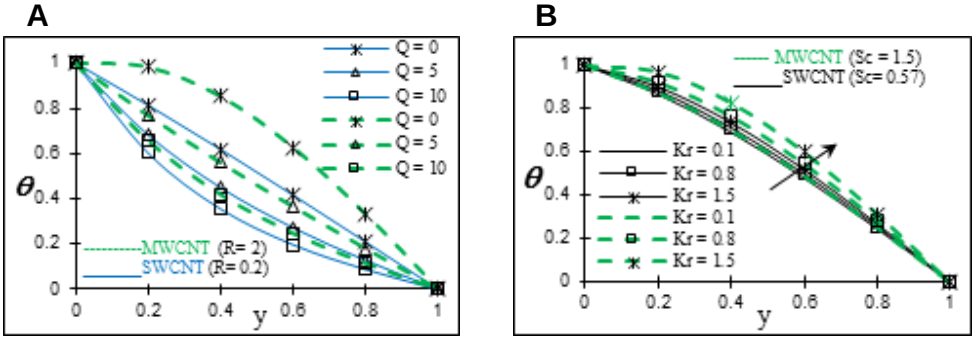

Fig. 6. A) Impact of Q on temperature profile (θ) for MWCNT (R = 2) and SWCNT (R = 0.2). B) Impact of Kr on temperature profile (θ) for MWCNT (Sc = 1.5) and SWCNT (Sc = 0.57).

In Fig. 6A, temperature depression has been seen for greater values of heat generation as the Q reduces the thermal boundary layer thickness, however temperature enhanced due to the impact of radiation. Interestingly, MWCNT is followed by the SWCNT substantially. Moreover, temperature of nanofluid is boosted without heat generation (Q = 0) for both the cases of MWCNT and SWCNT.

Fig. 6B depicts the behviour of chemical reaction (Kr) and Schmidt number (Sc) on temperature of nanofluid and it is observed that temperature enhances for large value of Kr and Sc. Due to the impact of MWCNT, the fluid temperature of nanofluid is greatest

for ethanol species (Sc = 1.5) in comparison with the Ammonia (Sc = 0.57) in SWCNT. In physical prospects, this behaviour is valid and always reverse to species concentration.

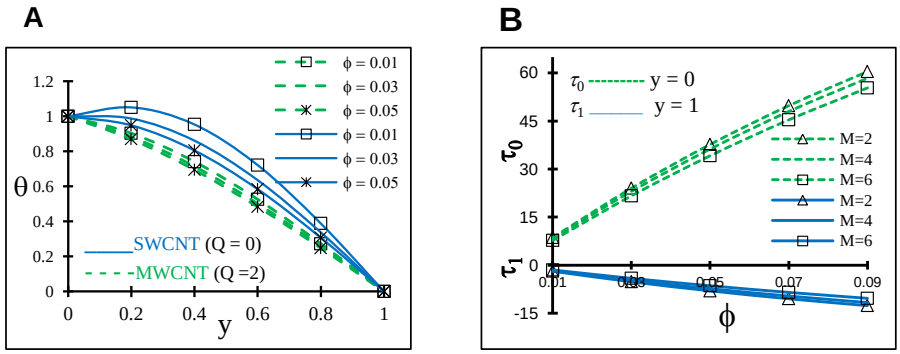

Fig. 7. A) Impact of ϕ on temperature profile (θ) for MWCNT (Q = 2) and SWCNT (Q = 0). B) Impact of ϕ and M on shear stresses at $y = 0$ and $y = 1$ walls for SWCNT.

In Fig. 7A, the effect of CNT volume fraction (ϕ) on temperature nanofluid in the case of SWCNT and MWCNT is presented. An increase in nanoparticle volume fraction reduces the temperature of MWCNT when Q = 5 and temperature is enhanced for SWCNT when Q = 0, which is opposite to MWCNT. This is due to the fact that the presence of heat generation diminishes the momentum and thermal boundary layers thickness.

In Fig. 7B, greater values of M reducing the shear stresses at the wall $y = 0$, whereas shear stresses becomes negative for the effect of M at the $y = 1$ wall and leads to more back flow during the motion in the carbon nanotubes. Opposite values are observed at both the walls and shear stresses are substantially increased for ϕ > 0.

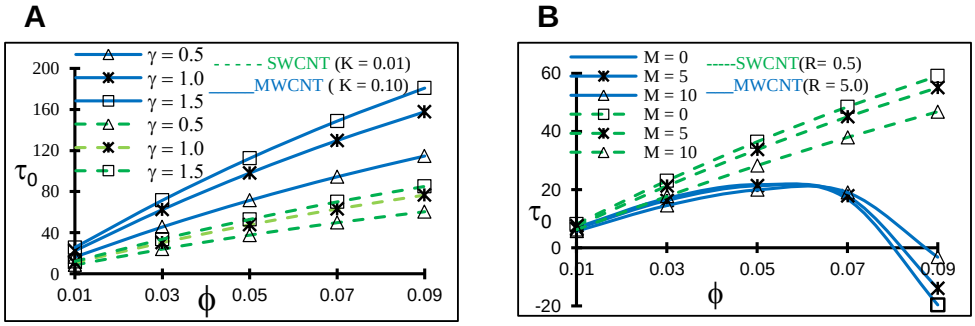

Fig. 8. A) Impact of ϕ and γ on shear stresses at $y = 0$ for MWCNT (K = 0.1) and SWCNT (K = 0.01). B) Impact of ϕ and M on shear stresses at $y = 0$ for MWCNT (R = 5.0) and SWCNT (R = 0.5).

Fig. 8A shows the behavior of ϕ and γ on shear stresses (τ_0) at $y = 0$ for CNTs when K = 0.1 and K = 0.01. Increasing porosity, CNT volume fraction and Casson parameter

boosted the values of shear stresses at the plate $y = 0$ and significantly MWCNT is more dominat than the SWCNT. In Fig. 8B, the behavior of drag force M supresses the shear stresses at the plate $y = 0$ for small radiation R = 0.5, while for higher radiation R = 10.0 there is a mixed behaviour for M that means after $\phi = 0.07$ the shear stresses gets reversed effect. Moreover, the CNT volume fraction enhanced τ_0 for R=0.5 and SWCNT is more dominant than the MWCNT in Fig. 8B.

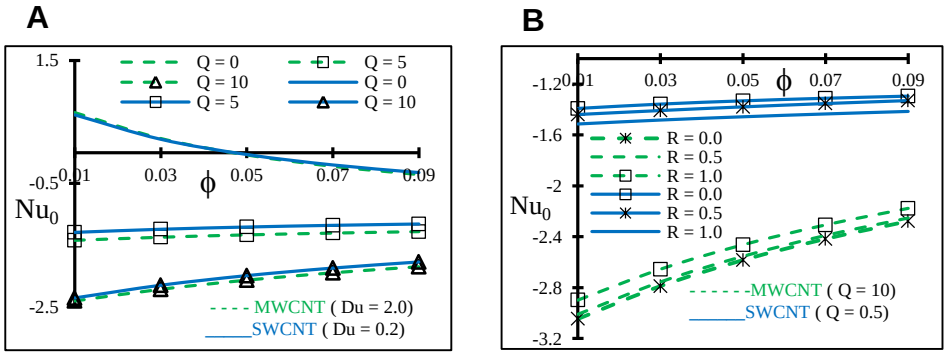

Fig. 9. A) Impact of ϕ and Q on Nu_0 at $y = 0$ for MWCNT (Du = 2.0) and SWCNT (Du = 0.2). B) Impact of ϕ and R on Nu_0 at $y = 0$ for MWCNT (Q = 10) and SWCNT (Q = 0.5).

The behavior of ϕ and Q on the rate of heat transfer (Nu_0) at $y = 0$ for different CNTs at Du = 2.0 and Du = 0.2 is presented in Fig. 9A. Increasing Q reduced Nu_0 and same effect is seen for Du. No effect has been observed at $Q = 5$ and maximum effect has occurred at $Q = 0$, Nu_0 has a reverse behavior without heat generation ($Q = 0$), but Nu_0 reduces for the CNT volume fraction. In Fig. 9B, the effects of ϕ and R on Nu_0 at $y = 0$ for $Q = 10$ and $Q = 0.5$ is displayed, here maximum effect has been occurred for the higher heat generation ($Q = 10$) than the lower $Q = 0.5$ which leads to the elevation of Nu_0 due to the effect of Q. Moreover, an asymptotic decay of Nu_0 has been occurred by the influences of CNT volume fraction and radiation. Here negative behavior of Nu_0 indicates that the heat is diffusing from Nanofluid particle to the plate $y = 0$. In magnitude of Nu_0, MWCNT has a dominant impact on the lower impact heat generation $Q = 0.5$.

5. Conclusion

The useful findings of hydromagnetic Casson (engine oil as base fluid) fluid in a vertical channel of porous medium for MWCNT's and SWCNT's with radiative heat transport are summarized as:

Engine oil-based CNTs has a great impact in the present research. At $R = 5$, a dominant behavior of SWCNT in nanofluid velocity has observed, but at $R = 0.5$, MWCNT shows reversed effect. The values of temperature of nanofluid for SWCNT at $Q = 0.5$ is heavier than that of MWCNT at $Q = 5$. However, the effects of heat generation on the

temperature distribution is similar in both the Figs. 6, 7 & 9. Moreover, it is observed that all the shear stresses at the plate $y = 0$ are positive means no opposite motion, while this behavior is reversed at the plate y = 1 means may occur opposite flow. Due to the influences of γ, ϕ, K, Gm and Gr, the fluid velocity is accelerated, but opposite trend is seen for M. The shear stresses are substantially increased for the augmented values of γ, ϕ, Du in CNT's, but opposite to the effect of M. Higher porosity gets the higher elevation of τ_0 for MWCNT. MWCNT has a heavier impact on Nu_0 for the higher $Q = 10$ than the lower $Q = 0.5$. Due to SWCNT, τ_0 elevated for CNT volume fraction for $R = 0.5$ and gets reversed for SWCNT for $R = 5.0$.

Appendix

$$\left\{\begin{array}{c}
\phi_1 = (1-\phi) + \phi\frac{\rho_{CNT}}{\rho_f}, \quad \phi_2 = \frac{1}{(1-\phi)^{2.5}}, \quad \phi_3 = 1 + \frac{3(\sigma-1)\phi}{(\sigma+2)-(\sigma-1)\phi}, \\
\phi_4 = (1-\phi) + \phi\frac{(\rho\beta)_{CNT}}{(\rho\beta)_f}, \quad \phi_5 = (1-\phi) + \phi\frac{\left((\rho C_p)_{CNT}\right.}{\left.(\rho C_p)_f\right.}, a_0 = \phi_1 Re \ , a_1 = \ \phi_2\left(1+\frac{1}{\gamma}\right), \\
a_2 = \left(\mathrm{M}^2\phi_3 + \frac{\phi_2}{\mathrm{K}}\right), \quad a_3 = \phi_4 \mathrm{Gr}, a_4 = \phi_4 \mathrm{Gm}, \quad a_5^2 = \frac{a_2}{a_1}, \\
a_6 = \frac{a_3}{a_1}, \quad a_7 = \frac{a_4}{a_1}, b_0 = \frac{\phi_5 \mathrm{Pe}}{\lambda_n}, \qquad b_1^2 = \frac{1}{\lambda_n}(\mathrm{R}^2 - \mathrm{Q}), \quad b_2 = \frac{\mathrm{Du}}{\lambda_n} \ , b_3^2 = (b_1^2 - \ b_0 i\omega), \\
d_1^2 \ = Sc.Kr, \qquad d_2 \ = Sc(i\omega + Kr), \lambda_1 = \frac{\lambda}{a_1}, \quad A = \frac{e^{-d_1}}{e^{-d_1} - e^{d_1}}, \quad B = \frac{-b_2 d_1^2 A}{d_1^2 + b_1^2}, \\
B_1 = \frac{-b_2 d_1^2 (1-A)}{d_1^2 + b_1^2}, \quad C_1 = 1 + B_1 - B, C = -B_1 e^{-d_1} + Be^{d_1} + C_1 cos(b_1), D = \frac{a_6 C}{(b_1^2 + a_5^2)}, \\
E = \frac{a_6 C_1}{(b_1^2 + a_5^2)}, \quad F = \frac{a_6 B}{(d_1^2 - a_5^2)}, G \ = \frac{a_6 B_1}{(d_1^2 - a_5^2)} - \frac{a_7(1-A)}{(d_1^2 - a_5^2)}, \qquad H = \frac{a_7 A}{(d_1^2 - a_5^2)}, \\
J = F + H, \qquad p_3 = \frac{1}{e^{a_8} - e^{-a_8}}\{1 - e^{a_8}\}\frac{\lambda_1}{a_8^2}, \quad p_1 = J - E - G, p_4 = -\frac{\lambda_1}{a_8^2} - p_3 \\
p_2 = \frac{1}{e^{-a_5} - e^{a_5}}\{Je^{d_1} - p_1 e^{a_5} - Dsin(b_1) - Ecos(b_1) - Ge^{-d_1}\}
\end{array}\right\} \quad (A.1)$$

References

1. W. A. Khan, Z. H. Khan, and M. Rahi, Appl. Nanosci. **4**, 633 (2014). https://doi.org/10.1007/s13204-013-0242-9
2. Q. Xue, Phys. B Condens. Matter. **368**, 302 (2005). https://doi.org/10.1016/j.physb.2005.07.024
3. R. Kandasamy, I. Muhaimin, and R. Mohammad, Alex. Eng. J. **55**, 275 (2016). https://doi.org/10.1016/j.aej.2015.10.006
4. T. Hayat, F. Haider, T. Muhammad, and A. Alsaedi, Int. J. Heat Mass Transfer, **112**, 248 (2017). https://doi.org/10.1016/j.ijheatmasstransfer.2017.04.123
5. Khalid, I. Khan, A. Khan, S. Shafie, and I. Tlili, Case Studies in Ther. Eng. **12**, 374 (2018). https://doi.org/10.1016/j.csite.2018.04.004
6. B. Mahanthesh, B. J. Gireesha, N. S. Shashikumar, and S. A. Shehzad, Physica E **94**, 25 (2017). https://doi.org/10.1016/j.physe.2017.07.011
7. S. Aman, I. Khan, Z. Ismail, Z., M. Z. Salleh, and Q. M. Al-Mdalla, Sci. Rep. **7**, 2445 (2017). https://doi.org/10.1038/s41598-017-01358-3
8. R. U. Haq, S. Nadeem, Z. H. Khan, N. F. M. Noor, and Phys. B Cond. Matter **457**, 40 (2015). https://doi.org/10.1016/j.physb.2014.09.031

9. N. Khan, S. Zuhra, Z. Shah, E. Bonyah, W. Khan, and S. Islam, AIP Adv. **8**, ID 115302 (2018). https://doi.org/10.1063/1.5055690
10. A. S. Khan, Y. Nie, Z. Shah, A. Dawar, W. Khan, and S. Islam, Appl. Sci. **8**, 2244 (2018). https://doi.org/10.3390/app8112244
11. S. Reddy, P. Sreedevi, and A. J. Chamkha, Pow. Technol. **307**, 46 (2017). https://doi.org/10.1016/j.powtec.2016.11.017
12. R. Kandasamy, T. Hayat, and S. Obadiah, Nuclear Eng. Design, **241**, 2155 (2011). https://doi.org/10.1016/j.nucengdes.2011.03.002
13. H. Hassan, Eur. J. Mechanics B/Fluids, **45**, 72 (2014). https://doi.org/10.1016/j.euromechflu.2013.12.003
14. S. Reddy and A. J. Chamkha, Adv. Powder Technol. **27**, 1207 (2016). https://doi.org/10.1016/j.apt.2016.04.005
15. N. Casson, Pergamon (New York, NY, USA, 1959).
16. S. Mukhopadhyay, K. Bhattacharyya, and T. Hayat. Chin. Phys. B. **22**, 114701 (2013). https://doi.org/10.1088/1674-1056/22/11/114701
17. E. M. Arthur, I. Y. Seini, and L. B. Bortteir, J. Appl. Math. Phys. **3**, 713 (2015).
18. T. Hayat, M. B. Ashraf, S. A. Shehzad, and A. Alsaedi, J. Appl. Fluid Mech. **8**, 803 (2015). https://doi.org/10.18869/acadpub.jafm.67.223.22995
19. S. Aman, I. Khan, Z. Ismail, M. Z. Salleh, A. S. Alshomrani, and M. S. Alghamdi, AIP Adv. **7**, 15036 (2017). https://doi.org/10.1063/1.4975219
20. H. C. Brinkman and M. Luis, J. Chem. Phys. **20**, 571 (1952). https://doi.org/10.1063/1.1700493
21. Y. Xuan, Q. Li, and W. Hu, AIChE J. **49**, 1038 (2003). https://doi.org/10.1002/aic.690490420
22. J. C. Maxwell and J. J Thompson (Oxford University Press, Oxford, UK. 1904).
23. A. S. Alsagri , S. Nasir, T. Gul, S. Islam, K. S. Nisar, Z. Shah, and I. Khan, Coatings **9**, 175 (2019), https://doi.org/10.3390/coatings9030175
24. Z. Iqbal, N. S. Akbar, E. Azhar, and E. N. Maraj, Euro. Phys. J. Plus **132**, 143 (2017). https://doi.org/10.1140/epjp/i2017-11406-0
25. A. Asadi, M. Asadi, A. Rezaniakolaei, L. A. Rosendahl, M. Afrand, and S. Wongwises, Int. J. Heat Mass Transf. 1**17**, 474 (2018).
26. Z. Shah, E. Bonyah, S. Islam, and T. Gul, AIP Adv. **9**, 15115 (2019). https://doi.org/10.1063/1.5048078
27. R. Haq, F. Shahzad, and Q. M. Al-Mdallal, Results in Phys. **7**, 57 (2017). https://doi.org/10.1016/j.rinp.2016.11.057
28. A. Zeeshan, N. Shehzad, R. Ellahi, and S. Z. Alamri, Neural Comput. Appl. **30**, 3371 (2018). https://doi.org/10.1007/s00521-017-2924-9
29. M. Saqib, F. Ali, I. Khan, N. A. Sheikh, and A. Khan, Arab. J. Sci. Eng. **44**, 1 **(**2019). https://doi.org/10.1007/s13369-018-3605-4
30. M. Saqib, I. Khan, and S. Shafie, Eur. Phys. J. Plus **133**, 549 (2018). https://doi.org/10.1140/epjp/i2018-12340-3
31. R. Ellahi, M. Raza, and N. S. Akbar, J. Porous Med. **20**, 461 (2017). https://doi.org/10.1615/JPorMedia.v20.i5.70
32. I. Khan and A. M. Alqahtani, Symmetry **11**, 378 (2019). https://doi.org/10.3390/sym11030378
33. G. C. Shit and S. Mandal, Int. J. Appl. Comp. Math. **6**, 2 (2020).
34. V. Choudhary and A. Gupta, Cabon Nanotubes-Polymer Composites (Intech Open Limited 5 Princes Gate Court, London, SW7 2QJ, UK, 2011). https://doi.org/10.5772/18423
35. B. Ribeiro, E. C. Botelho, M. L. Costa, and C. F. Bandeira, Polimeros **27**, 247 (2017). https://doi.org/10.1590/0104-1428.03916
36. D. Kalita, S. Hazarika, and S. Ahmed, JP J. Heat Mass Trans. **20**, 105 (2020). https://doi.org/10.17654/HM020020105
37. D. Kalita, S. Hazarika, and S. Ahmed, ANNALS of Faculty Eng. Hunedoara – Int. J. Eng. **18** (2020).

38. Y. Menni, A. J. Chamkha, N. Massarotti, H. Ameur, N. Kaid, and M. Bensafi, Int. J. Num. Methods Heat Fluid Flow **30** (2020). https://doi.org/10.1108/HFF-10-2019-0739
39. M. Y. Arafat and F. Faisal, J. Sci. Res. **12**, 499 (2020). https://doi.org/10.3329/jsr.v12i4.45605